Acoustic remote sensing of internal solitary waves and internal tides in the Strait of Gibraltar

Christopher O. Tiemann,[a] Peter F. Worcester, and Bruce D. Cornuelle
Scripps Institution of Oceanography, University of California at San Diego, La Jolla, California 92093

(Received 20 July 2000; revised 26 February 2001; accepted 27 April 2001)

High-frequency underwater acoustic transmissions across the Strait of Gibraltar are used to examine the feasibility of acoustically measuring several physical processes in the Strait, a difficult area to sample with conventional instruments. Internal undular bores propagate along the interface between an upper layer of Atlantic water and a lower layer of Mediterranean water. As they cross the acoustic path they are recognized by their scattering effects in the acoustic record. The time between internal bore crossings is influenced more by the tidal phase of the bore release at the Camarinal Sill than by variability in the bore's propagation time to the acoustic path. When internal bores were present, the acoustic arrival patterns could be classified as one of three types with different internal bore and internal tide amplitudes. The arrival types alternate during spring to neap tide transitions, suggesting that internal bore amplitude is not linearly related to tidal height. The sensitivity of acoustic observables to several physical parameters is investigated using a forward model, and a demonstration of inverse techniques provides estimates of several physical parameters from spring tidal cycles. © *2001 Acoustical Society of America.* [DOI: 10.1121/1.1382617]

PACS numbers: 43.30.Pc, 43.30.Cq [DLB]

I. INTRODUCTION

The Strait of Gibraltar is a challenging environment to observe with conventional instruments. Its large variability over small time and space scales makes it difficult to sample adequately, and the strong tidal currents and extensive ship and fishing traffic there are inhospitable to moored instruments. CTD casts and moorings have provided most historical information about internal tides in the Strait (Armi and Farmer, 1988; Farmer and Armi, 1988; Boyce, 1975; Bray *et al.*, 1990, 1995; Candela *et al.*, 1990; Ziegenbein, 1970), but CTD data can suffer from temporal aliasing problems because of the brevity of some important physical processes in the Strait. While moored instruments can sample quickly, they are point measurements subject to spatial aliasing and contamination from local, small-scale variability.

Packets of large internal solitary waves routinely propagate west through the Strait and have received considerable attention (Boyce, 1975; Watson, 1994; Watson and Robinson, 1990; Ziegenbein, 1970). These solitary waves are difficult to observe using CTD measurements because of their short duration at any one point. Satellite and surface radar images have been successful in observing their speed and horizontal wave-front shape but give no indication of their vertical structure (Alpers and La Violette, 1993; Richez, 1994; Watson, 1994; Watson and Robinson, 1990). Echosounders have successfully observed the vertical displacement of internal solitary wave packets (Armi and Farmer, 1988; Farmer and Armi, 1988; Watson, 1994), but the variability of their shape with range across the Strait has not been directly observed.

Although conventional measurement techniques are suitable in some situations, they all have limitations in the environment of the Strait of Gibraltar. A technique that has received less attention in the Strait, yet offers some advantages over conventional methods, is that of acoustic remote sensing. A key virtue of using acoustics is the ability to make rapidly repeated measurements which eliminates any problems of aliasing in time. Acoustic transmissions across the Strait of Gibraltar are practically instantaneous relative to the time scales of even the briefest physical processes. Acoustic measurements inherently integrate horizontally, which suppresses small-scale variability, and they can even be used to measure several parameters simultaneously, as this work will show.

The Strait of Gibraltar Acoustic Monitoring Experiment was conducted in April 1996 as a joint project between the Scripps Institution of Oceanography and the Institut für Meereskunde, University of Kiel. The Gibraltar experiment has already provided acoustically derived estimates of transport through the Strait (Send *et al.*, 2001), but this paper provides examples of additional information that can be sensed acoustically and offers new insight into the interesting physical processes in the Strait. The potential exists to learn much about the physical oceanography in the Strait without deploying extensive instrumentation in its interior.

Tiemann *et al.* (2001) investigated the scattering effects of internal solitary waves and internal tides on acoustic transmissions across the Strait of Gibraltar by using a multiparameter physical model of the Strait in the forward problem. This model can qualitatively explain many important features of the observed acoustic scattering by showing how acoustic ray paths across the Strait evolve over a tidal cycle. The same model was further used in this work to determine how sensitive acoustic travel times are to changes in several physical parameters such as internal solitary wave amplitude, internal solitary wave speed, and internal tide amplitude.

[a]Now at: Science Applications International Corporation, La Jolla, CA 92037.

 0001-4966/2001/110(2)/798/14/$18.00

This paper will demonstrate three different techniques for extracting oceanographic information from an acoustic record. These analyses are independent of each other and will each appear in their own section, ordered in increasing complexity. Section II provides a general overview of the environment of the Strait of Gibraltar, the experiment instrumentation, and the physical model used in the forward problem. Section III shows an example of how acoustics can be used to determine when internal solitary waves are present and, when used in conjunction with conventional measurements, to time the travels of internal bores through the Strait. In Sec. IV, three generalized acoustic travel time arrival patterns are identified. These patterns are repeated frequently in the acoustic record, and their sequence shows some interesting long term trends. In Sec. V, the sensitivity of acoustic propagation in the Strait to perturbations in the physical model parameters is examined, and in some cases a qualitative explanation for the resulting travel time changes is provided. Following this is a description of the linear inverse technique used to estimate several physical parameters from the acoustic data.

II. OVERVIEW

An understanding of the physical processes in the Strait of Gibraltar is necessary for modeling acoustic propagation in the region. Tiemann *et al.* (2001) describe in detail the model previously developed to describe the oceanographic processes in the Strait and aid in acoustic propagation studies, but key features of the environment, experimental approach, and model parameters are repeated briefly here.

The basic circulation of the Strait is relatively simple, with an upper layer of relatively warm, fresh Atlantic water about 100 m thick flowing east into the Mediterranean Sea and a lower layer of relatively salty, cold Mediterranean water flowing back west through the Strait into the Atlantic. This mean flow is modulated by large semidiurnal tidal flows, and there are tidal fluctuations in the depth of the interface between the upper Atlantic and lower Mediterranean water layers. Within the model, these fluctuations from the internal tide are reproduced by sinusoidal vertical shifts of the background sound-speed field of up to 25 m on the northern side of the Strait and 40 m on the southern side.

Perhaps the most interesting feature, though, is the propagation of internal bores which are released at the Camarinal Sill on the west side of the Strait at the relaxation of most high tides. As the bore propagates east through the Strait it eventually disintegrates into a train of internal solitary waves, with waves of larger amplitude and wavelength at the head of the packet. Within the model, the vertical amplitude of the internal solitary wave packets is based on an echosounder observation of a packet near the acoustic path but is scaled with position across the Strait, increasing from north to south, with an average 100 m amplitude near the center of the Strait. The modeled packet crosses the experiment's acoustic path with a speed of 2.5 m/s and with a horizontal wave-front curvature based on one observed in a satellite image.

The geometry of the Gibraltar experiment was selected to give both lower acoustic ray paths across the Strait that were confined to the lower layer of Mediterranean water and upper ray paths that acoustically sampled the interface between Atlantic and Mediterranean waters and the internal solitary waves which propagate along that interface. Three 2 kHz transceivers (labeled T1, T2, and T3 in Fig. 1) were installed just above the sea floor at about 200 m depth, at the endpoints of two acoustic paths. Transmissions every 2 min from T1 to T3 will be examined in this paper; the T1–T3 path was perpendicular to the current flow to minimize any acoustic travel time variation due to currents. The tilts and orientations of the instrument moorings were measured every 5 min and used to correct acoustic travel times for instrument motion, but close examination of the T1 instrument tilt data showed brief but violent tilts occurring roughly every 12 h. These ''kicks'' are due to the passing of an internal solitary wave over the instrument and provide a hint as to where to look in the acoustic data for internal solitary wave effects.

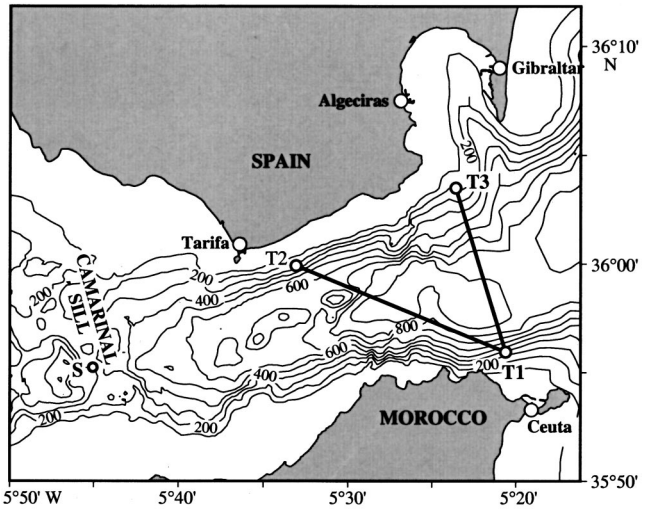

FIG. 1. Bathymetry of the Strait of Gibraltar with instrument positions and acoustic paths indicated. Due to inaccuracies in bathymetry, depth contours do not exactly match instrument depths.

The observed acoustic scattering was quite complicated as ray paths were repeatedly created and destroyed with the passing of internal solitary waves and the evolution of the internal tide. The background sound-speed field used in the model was constructed from environmental data taken during the experiment and has double minimums in the sound-speed profiles at every range. Within the model, the sound-speed field is shifted vertically and adiabatically in accord with a mode 1 internal tide. Furthermore, when an internal solitary wave crosses the acoustic path, it temporarily displaces warm shallow water deeper, perturbing the sound-speed profiles even further. The internal solitary wave is modeled as another mode 1 vertical displacement which sharpens sound-speed gradients. The increased sound-speed gradients can then refract acoustic rays away from their usual sound channels. To illustrate this, Fig. 2 shows absolute acoustic travel times to the T3 instrument over two tidal cycles, and Fig. 3 shows the predicted ray paths and soundspeed field along the T1–T3 acoustic path at several instances in a tidal cycle. The ray identifiers (''a'' through ''e'') of Fig. 3 correspond to the same labels on the travel times of Fig. 2. Ray path ''a'' will be referred to as the ''lower ray'' because it consistently

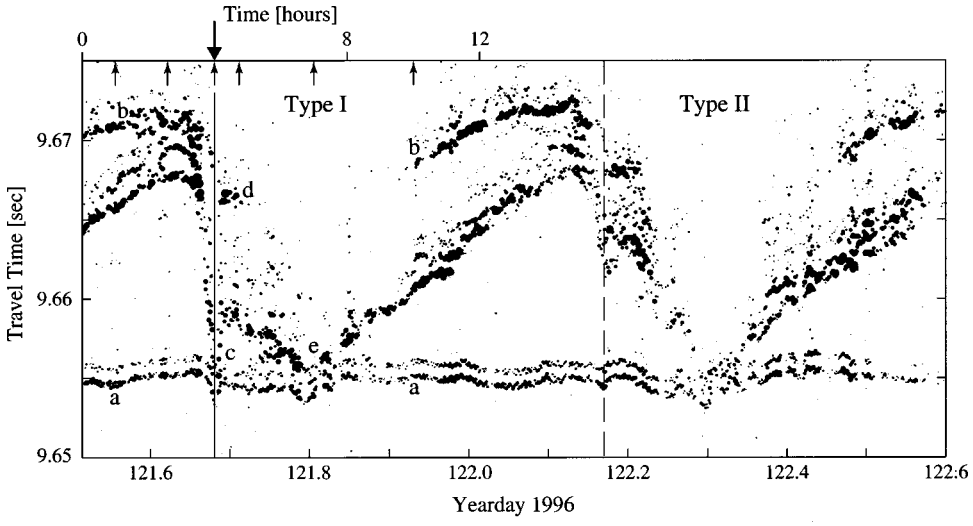

FIG. 2. Absolute travel times as a function of yearday 1996 for transmissions from T1 to T3. Each arrival peak is plotted as a dot, with size proportional to SNR. Vertical lines indicate times of internal bore crossings and arrival structure type (Type I solid, Type II long dash). Labels "a" through "e" identify key features of the acoustic data which were matched in the predicted data and correspond to the ray identifiers of Fig. 3. Small arrows indicate times for which ray paths are shown in Fig. 3. Large arrow indicates time of a large tilt of the T1 instrument. Type I and II arrival structure labels are described further in Sec. IV.

sampled the lower water layer. Its travel time of 9.655 s is nearly constant throughout the tidal cycle. Ray paths "b" through "e" will collectively be called "upper rays," and they showed much more travel time variability, such as the rapid 15 ms decrease in travel time near Hour 4 of Fig. 2. Despite such complexity, the acoustic scattering is surprisingly robust, and the repeatability of key acoustic features made the Gibraltar data set a good candidate for modeling.

III. INTERNAL BORE TRAVEL TIME

The internal undular bores in the Strait of Gibraltar originate at the Camarinal Sill to the west. A lee wave in the form of an internal hydraulic jump appears behind the sill during strong westward tidal flows. When the tide relaxes, this wave is free to cross the sill and moves east as an internal bore along the interface between the Atlantic and Mediterranean waters. Using temperature and salinity records from several moorings along the main axis of the Strait, Armi and Farmer (1988) timed the passage of a mode 1 internal bore through the Strait; they predict the bore should cross the Gibraltar experiment's T1–T3 acoustic path approximately 5.5 h after its release from the Camarinal Sill. Acoustic data can also be used to time the passing of a bore over the acoustic path because its scattering effects in the acoustic record are recognizable. Note that by that time, the bore will have evolved into a packet of internal solitary waves.

As an internal solitary wave train crosses the T1–T3 acoustic path the travel times for both upper and lower eigenray paths should decrease sharply as they are refracted down deep due to large sound-speed gradients at the source. This ray path refraction is illustrated in Fig. 3, Hour 4. The horizontal wave-front curvature of the solitary wave packet prevents discrete oscillations for each solitary wave from appearing in the acoustic record (Tiemann *et al.*, 2001). The severity of the travel time drop varies with the vertical amplitude of the passing internal solitary waves; larger waves cause larger sound-speed gradients and steeper ray path refractions. Such rapid drops in travel time are often seen in the acoustic data, once per tidal cycle, and they coincide with the violent kicks seen in the T1 instrument's tilt data. (The 10–15 ms travel time decrease for upper ray paths is not the result of instrument motion.) However, not every abrupt travel time decrease has a corresponding indicator in the instrument's motion data. The data from both semidiurnal tidal cycles of Fig. 2 show sharp decreases in travel time, at yeardays 121.68 and 122.17, indicative of an internal solitary wave packet crossing the acoustic path, but the acoustic data suggest that the earlier packet at day 121.68 has a bigger amplitude because the travel time decrease of the upper rays is larger (15 ms drop vs 10 ms drop). The T1 instrument motion confirms a larger internal solitary wave at day 121.68 as a violent tilt was recorded at the instrument, moored at a depth of 165 m, but not in the later case when smaller amplitude waves did not extend deep enough to move the instrument.

A sudden travel time decrease is the acoustic signature of a passing internal solitary wave, and for every tidal cycle where one occurred, the yearday at the maximum decrease was noted as the time of the internal solitary wave crossing. Not every tidal cycle has an associated crossing, particularly during neap tides when the internal bores are smaller in amplitude or nonexistent. Figure 4(a) shows the spacing in time, as a function of yearday, between internal bores crossing the acoustic path; spacings between bores more than one tidal cycle apart are not considered here. The tidal height record from Ceuta is shown beneath to illustrate days of spring and neap tides and the tidal daily inequality. The mean time between bore occurrences is 12.56 h, but their spacing oscillates shorter or longer than the mean on consecutive tides. The bore spacing also seems to vary more with the size of the tidal daily inequality than with overall tidal amplitude; Figure 5 suggests a roughly linear relationship between the time separating two internal bore occurrences and the difference in low tide heights from their tidal cycles. For the tidal record shown in Fig. 4(d), the time between consecutive high tides varies up to $\pm.7$ h, usually alternating above and below the mean period of 12.46 h. This variation in tidal period helps account for part of the ± 3.5 h maximum variation in bore spacings. The remaining variation could be due to changes in a bore's release time from the Camarinal Sill, relative to high tide, or to differences in some physical prop-

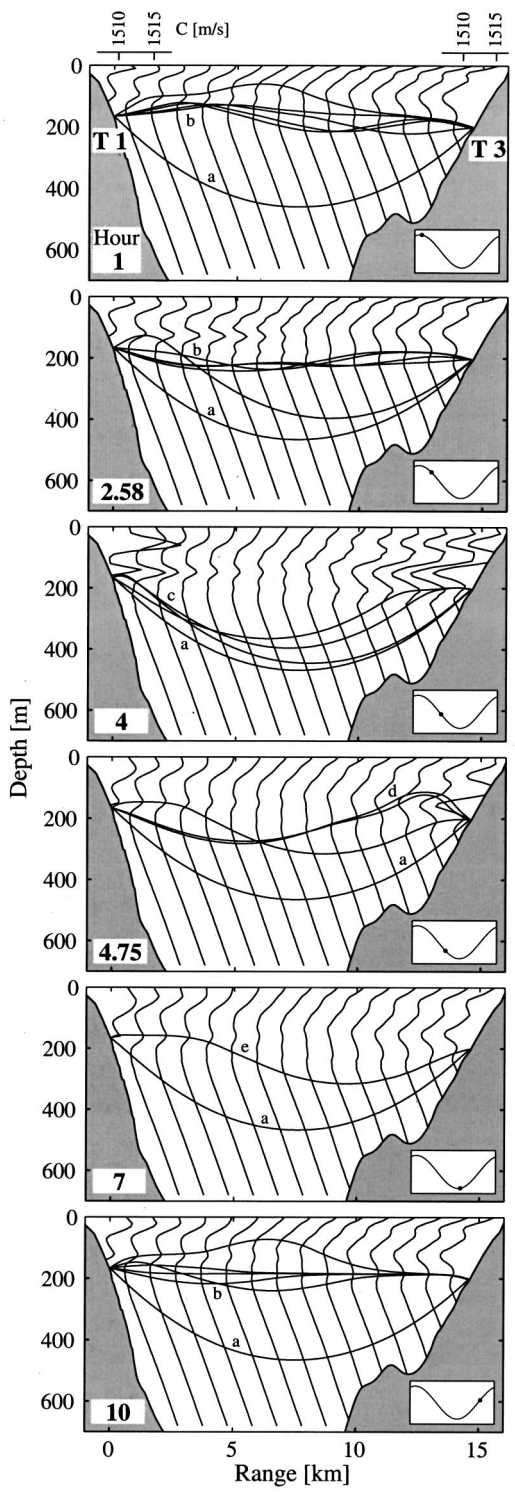

FIG. 3. Vertical sections along the T1–T3 acoustic path showing background sound-speed profiles and predicted ray paths at several times in a 12 h spring tidal cycle. Inset shows phase within the tidal cycle. The view is looking west with the southern T1 source on the left. The ray identifiers (''a'' through ''e'') correspond to the same labels of Fig. 2. Scale for profile values is the same for all profiles but offset in range. This figure is reproduced from Tiemann *et al.* (2001).

erties such as the bore's phase speed or currents in the Strait.

Determining a bore's release time from the Camarinal Sill is necessary in calculating its travel time to the acoustic path and its phase in the tidal cycle. To do so in this experiment, conventional instruments were essential. It is difficult

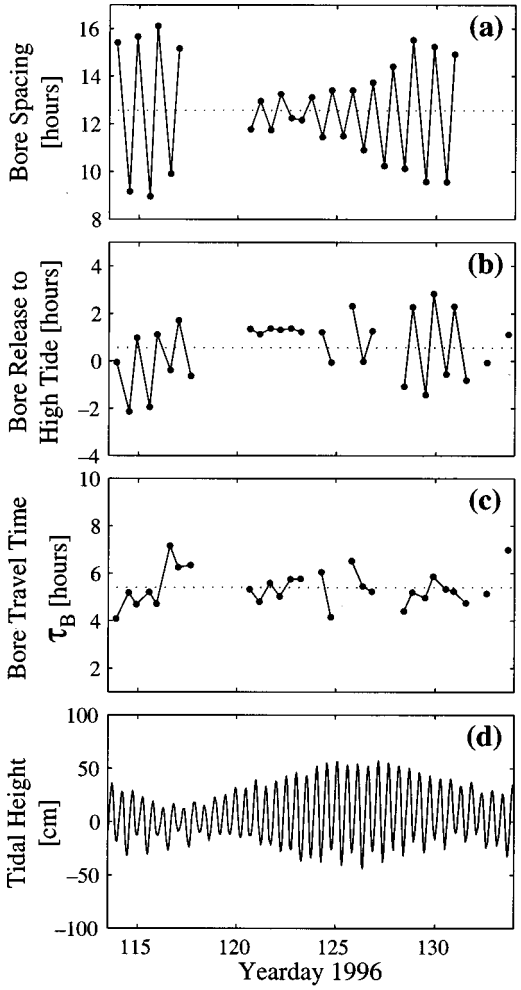

FIG. 4. (a) Time between internal bore crossings separated by no more than one tidal cycle. (b) Time from a bore release to the nearest high tide at Ceuta. Positive values indicate a bore release prior to the high tide. (c) τ_B, bore travel time from the Camarinal Sill to the acoustic path. In (a) through (c), data points from adjacent tidal cycles are connected by a line. The mean is shown as a dotted line. (d) Tidal height record from Ceuta.

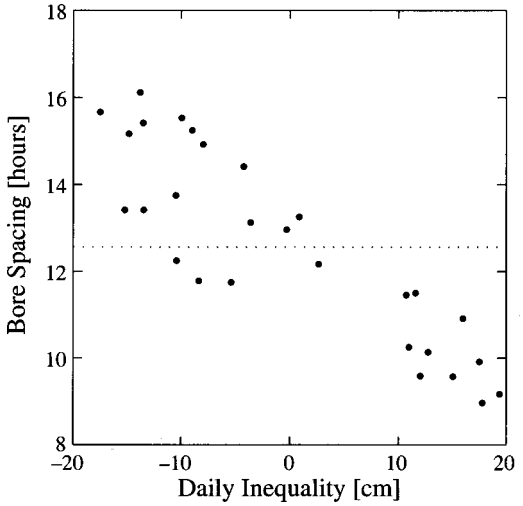

FIG. 5. Time between internal bore crossings vs the tidal daily inequality at Ceuta for yeardays 114 to 135. The daily inequality is the difference in tidal height between adjacent low tides. Dotted line indicates the mean internal bore spacing of 12.56 h.

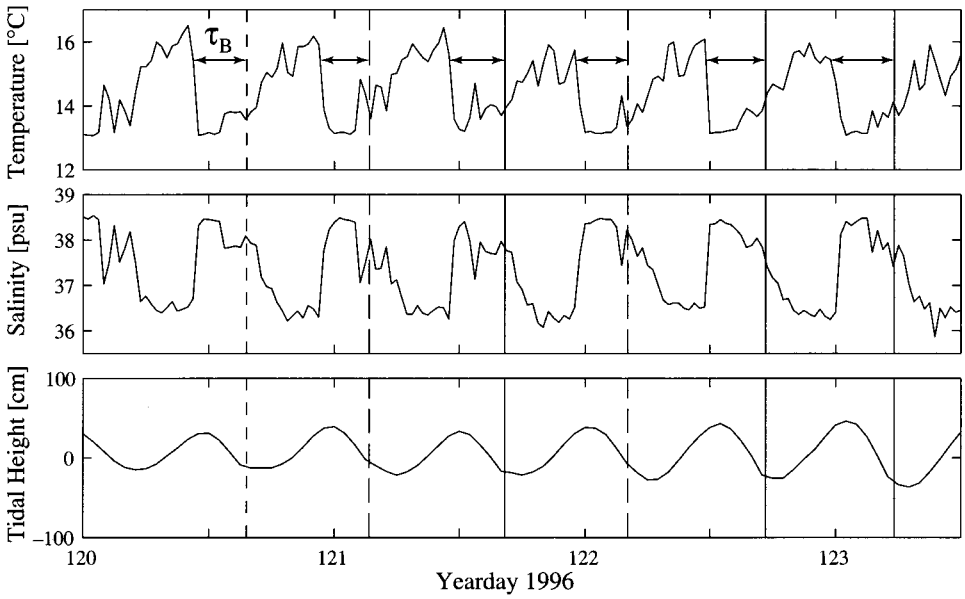

FIG. 6. Temperature and salinity records from 118 m depth at mooring "S" on Camarinal Sill, plus the tidal height record from Ceuta, for six tidal cycles. Vertical lines indicate times of internal bore crossings at the acoustic path and arrival structure type (Type I solid, Type II long dash, Type III short dash). The bore's travel time, τ_B, is dimensioned six times in the temperature series. The complete time series for τ_B is shown in Fig. 4(c).

to estimate the time of a bore's release using current meter data from the sill because of uncertainties in how strong a current is necessary to hold a bore in place. Instead, abrupt changes in the temperature and salinity record from the sill are a better indicator of an internal bore release. Figure 6 shows the temperature and salinity record at 118 m depth from the sill mooring (labeled "*S*" in Fig. 1). Data from six consecutive tidal cycles are shown, with the tidal height at Ceuta provided for reference. The vertical bars on the figure indicate times of internal bore crossings at the acoustic path as determined from the acoustic data. Approximately 5 h before each bore crossing, there is a rapid drop in temperature at the sill of about 3 °C and a simultaneous rise in salinity of about 2 psu; this event designates the time of the bore release. The clearest examples of bore releases are shown in Fig. 6, however, the temperature and salinity records were not consistently good markers. In ambiguous cases where there was no sharp temperature or salinity change, no attempt was made to time the bore release.

The time from all bore releases to their nearest high tide in the tidal record is shown in Fig. 4(b). The bore was released an average of 34 min before the high tide, but release can occur over 2 h before or after the high tide, often alternating above and below the mean on successive tidal cycles. This series is another example where the bore's characteristics are steadiest during days of small daily inequalities. Armi and Farmer (1988) observed a 1 h variation in the tidal phase of the bore release and also attributed this to the diurnal inequality in the tide.

The travel time for an internal bore to propagate from the Camarinal Sill to the acoustic path is the difference between a bore's release time and the time of its crossing as determined from the acoustic data. This quantity is labeled in Fig. 6 as τ_B and its time series is shown in Fig. 4(c). The mean bore travel time is 5.4 h, and this is in agreement with Armi and Farmer's measurement of 5.5 h along the same path (1988). The time series for bore travel time is considerably less variable than that of the bore's tidal phasing, with rms values of 0.76 and 1.31 h, respectively. The variation in the time between internal bore arrivals is influenced more by variability in the tidal phase of the bore release than by variability in the bore's travel time.

IV. ARRIVAL PATTERN IDENTIFICATION

The repeatability of key features in the acoustic data during spring tidal cycles is what made the Gibraltar data set such a good candidate for modeling attempts, and the model developed previously (Tiemann *et al.*, 2001) successfully reproduced many properties of the acoustic arrival pattern for spring tides. The data set shows robustness outside of the spring tides as well. Examination of acoustic data during the transitions between spring and neap tides reveals that there are two more broad categories of arrival structures, repeated often and usually on alternating tidal cycles.

The acoustic data from the three consecutive tidal cycles shown in Fig. 7(a) were used as archetypes for classifying arrival structures according to their distinguishing characteristics. The three arrival structures will be identified simply as Type I, II, and III, and their key features are listed in Table I and labeled on the dot plot of Fig. 7(a). The times of an internal bore crossing the acoustic path are indicated by vertical lines where the line type (solid, long dash, short dash) corresponds to the classification of the arrival pattern (Type I, II, or III) for that tidal cycle. The analysis to follow takes advantage of the qualitative differences among arrival patterns as listed in Table I. A later section will quantitatively examine the features of Type I arrivals.

Note that after yearday 128.0, the acoustic travel times will appear shifted 15 ms earlier [compare Figs. 2 and 7(a)] because the T1 instrument autonomously redeployed itself about 23 m closer to the T3 receiver. As mentioned earlier, the Strait of Gibraltar is a difficult environment for moored instruments! That shift will not adversely affect this work as only relative travel time changes are of interest, and the eigenray paths predicted by the model are essentially the same for the new, slightly shorter acoustic path.

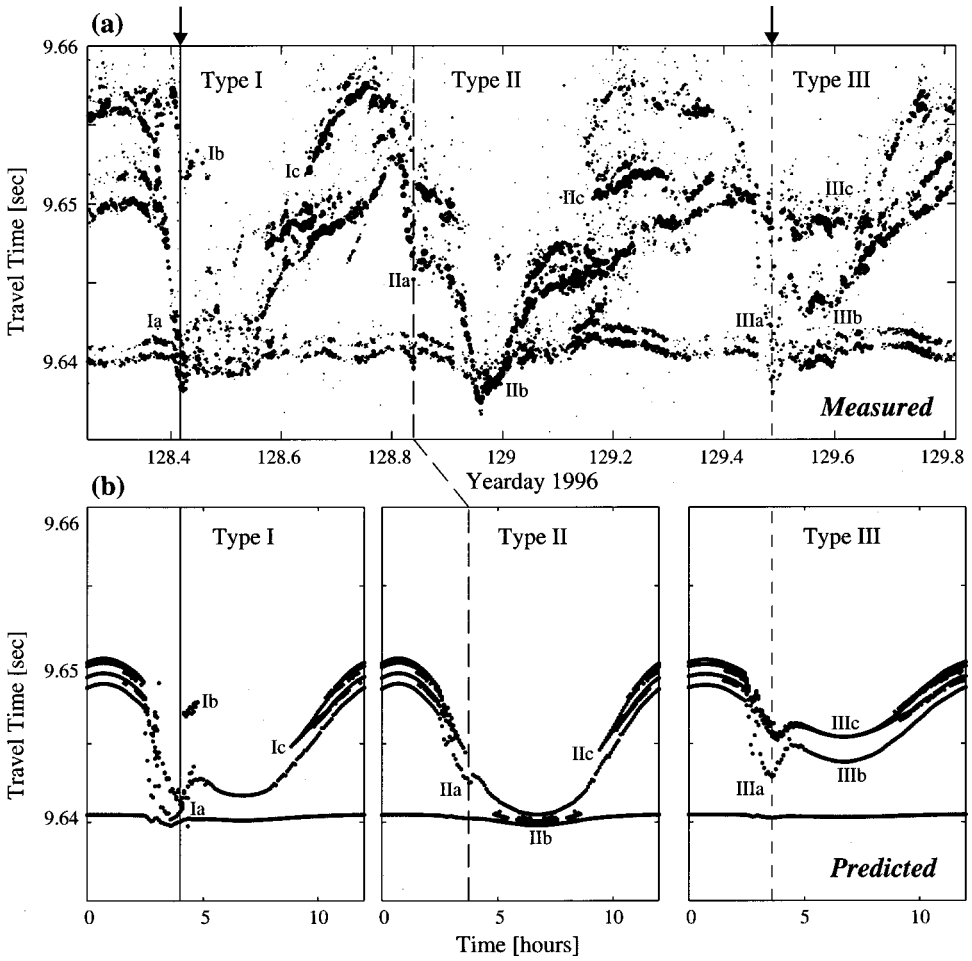

FIG. 7. Measured and predicted ray travel times over three tidal cycles. The labels (''Ia'' through ''IIIc'') identify key features of the measured data matched by the model output and are described in the text and in Table I. Vertical lines indicate times of internal bore crossings and arrival structure type (Type I solid, Type II long dash, Type III short dash). Arrows indicate times of a large tilt of the T1 instrument.

The three tidal cycles of Fig. 7(a) are from a transition period from spring to neap tides. The Type I arrival structure shows the last of spring tides; reproducing this structure was the goal of the first modeling attempts. By changing some model input parameters, key features of the Type II and Type III arrival structures can be reproduced as well, providing an understanding of the relative changes in physical processes between the different arrival types. Figure 7(b) shows predicted travel times for three tidal cycles as output by the model in attempts to match the three types of arrival structures. Although the key features listed in Table I were qualitatively reproduced by the models, other details of the measured data are not reproduced. This is mainly due to errors in the background sound-speed field as environmental data were limited during sound-speed profile construction. Attempts to more closely match the travel time separation between lower and upper ray arrivals (''a'' and ''b'' of Fig. 2) by ''speeding up'' the lower water layer and ''slowing down'' the upper water layer complicated other ray paths beyond what is seen in the data. Although the model for Type I arrivals does not exactly reproduce the observed travel times, its model parameters are suitable for use as a reference state in the sensitivity studies to follow.

TABLE I. Features of travel time arrival patterns.

Feature		Description
Type I	Ia	Sudden upper ray travel time decrease of about 15 ms.
	Ib	Isolated cloud of upper ray arrivals shortly after bore crossing.
	Ic	Absence of late-arriving upper rays for several hours.
Type II	IIa	Sudden upper ray travel time decrease of about 10 ms.
	IIb	Upper ray travel times continue to decrease following bore crossing.
	IIc	Absence of late-arriving upper rays for several hours.
Type III	IIIa	Sudden upper ray travel time decrease of 10–15 ms.
	IIIb	Lower and upper ray arrivals separated through most of tidal cycle.
	IIIc	Late-arriving upper rays present through entire tidal cycle.

The model parameters used to match the Type I case are described in Sec. II and in detail in Tiemann *et al.* (2001). When matching the Type II case, the internal bore amplitude was reduced to 20% of the reference case; this prevents the initial upper ray travel time decrease from being so severe (feature ''IIa'' from Table I) and allows the late-arriving upper rays to persist longer before disappearing (''IIc''). The continued drop in upper ray travel times, reaching a minimum in the middle of the tidal cycle (''IIb''), is more likely the result of internal tides vertically shifting the background

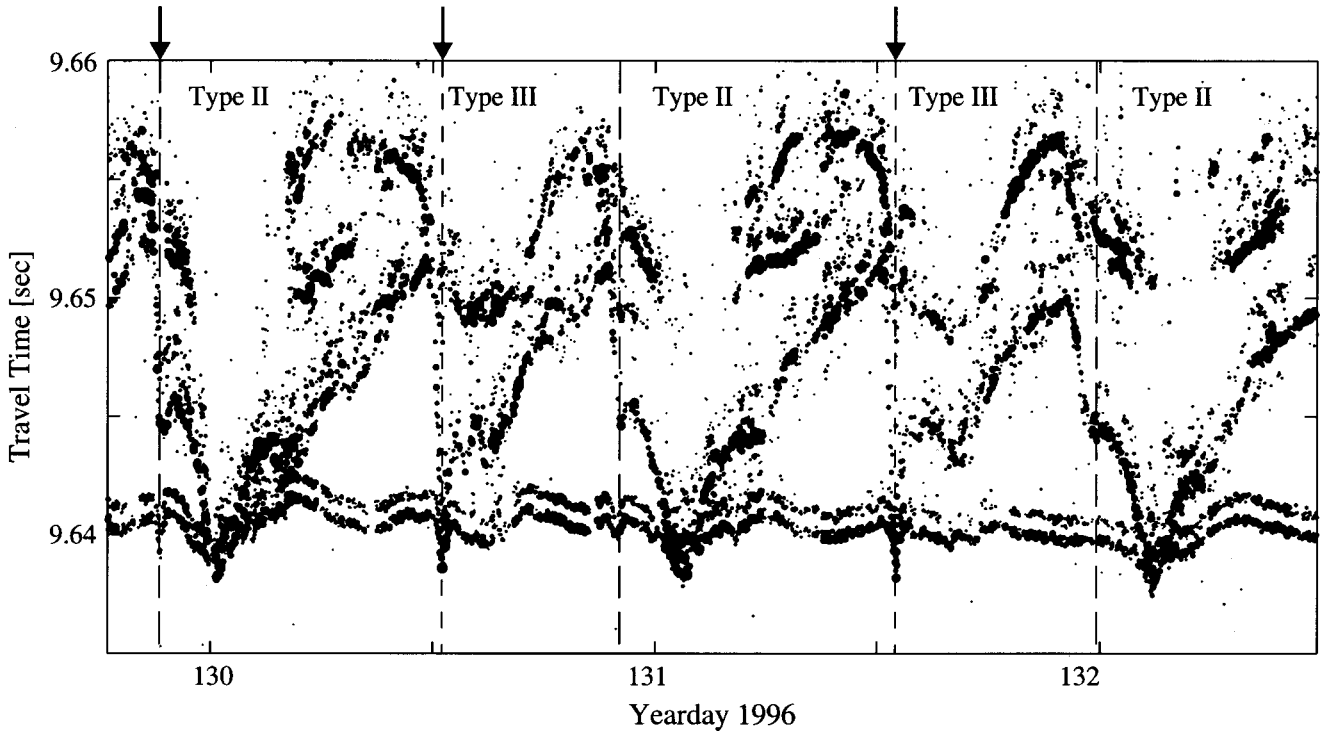

FIG. 8. Absolute travel times for five tidal cycles as a function of yearday 1996 for transmissions from T1 to T3. Vertical lines indicate times of internal bore crossings and arrival structure type (Type II long dash, Type III short dash). Arrows indicate times of a large tilt of the T1 instrument.

sound-speed field rather than internal solitary wave effects. Thus internal tide amplitude was increased slightly by 10 m, and the background sound-speed profiles were uniformly shifted deeper by 10 m in order to minimize the lower/upper ray travel time separation at the bottom of the tidal cycle. Offsetting the background sound-speed profiles from their reference state is equivalent to changing the depth of the Atlantic/Mediterranean interface, which could reasonably be varying from one tidal cycle to the next. Furthermore, shifting the sound-speed field slightly is not unreasonable given the uncertainties in the range-dependent sound-speed field construction.

Because the variation in upper ray travel times for the Type III case is smaller and the lower/upper ray travel time separation larger, the opposite model parameter change was made: internal tide amplitude was decreased by 12 m and the background sound-speed field was shifted shallower by 10 m. Shifting the background sound-speed field shallower maintains late-arriving upper rays throughout the entire tidal cycle (''IIIc''). The internal solitary wave amplitude in the Type III case is decreased to 30% of the reference state in order to provide an initial upper ray travel time decrease of a size between the Type I and Type II cases (''IIIa'') but yet not be so large that the late-arriving upper ray paths disap-

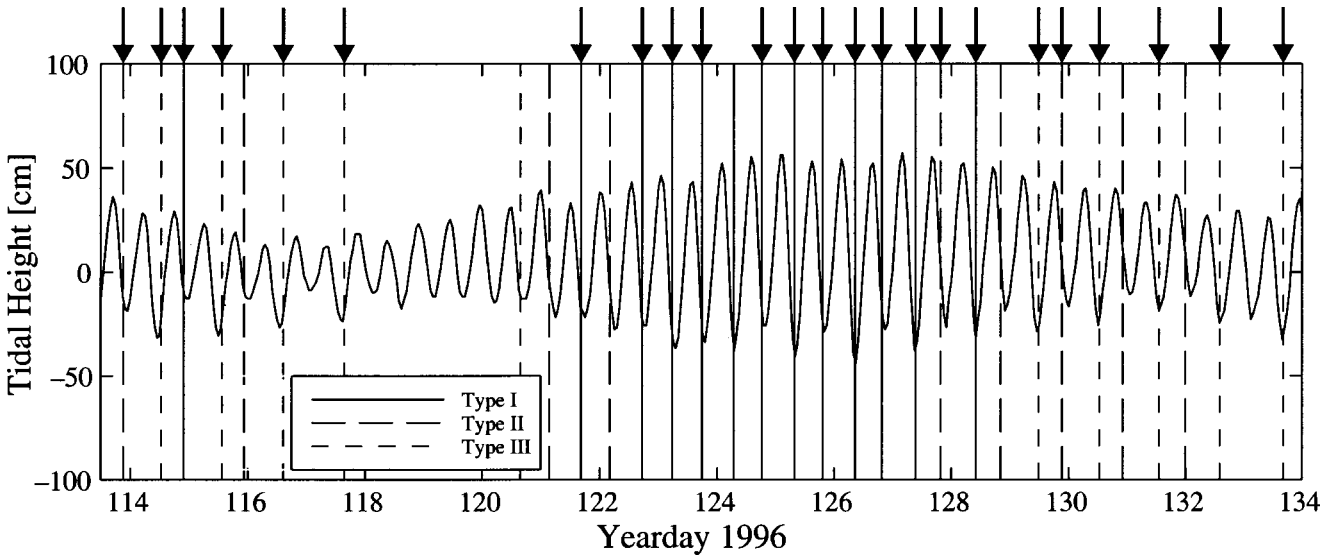

FIG. 9. Tidal height at Ceuta as a function of yearday 1996 overlaid with vertical lines indicating times of internal bore crossings and arrival structure type (Type I solid, Type II long dash, Type III short dash). Arrows indicate times of a large tilt of the T1 instrument.

pear. In summary, the Type I arrivals assume the largest internal solitary wave amplitude. The Type II arrivals use the smallest internal solitary wave amplitude but the largest internal tide amplitude. The Type III arrivals assume a middle-sized solitary wave, but the smallest internal tide.

Every tidal cycle where an internal bore crossing was seen was catalogued as one of the three types of arrival structures shown in Fig. 7(a). Although this was done by a visual pattern matching, there was usually little doubt as to which archetype most closely resembled each tidal cycle's arrival structure. For example, note how the presence of late arriving upper rays in a Type III arrival (feature IIIc) distinguish it from Types I and II where those rays are absent. Additionally, in a Type II arrival, the convergence of upper and lower ray travel times happens hours after the initial upper ray travel time decrease (feature IIb), distinguishing it from Types I and III. Figure 8 shows acoustic data from five more tidal cycles where alternating Type II and Type III arrival structures are relatively obvious. Again, the vertical bars in this figure indicate times of an internal bore crossing, and arrows indicate an accompanying severe tilt in the T1 instrument. As additional examples, the travel times of Fig. 2 would be classified as a Type I and Type II arrival (Fig. 10 is a Type I arrival).

After classifying all of the tidal cycles with bore occurrences by arrival type, an interesting pattern emerged when plotting arrival type on a tidal height record from Ceuta. Figure 9 shows times of internal bore crossings as vertical lines where line type distinguishes arrival type. The tidal record identifies days of spring and neap tides and the daily inequality. Note how Type I arrivals, modeled with the largest internal bore amplitude, occur during the spring tides, while Type II and Type III arrivals are seen on days to either side of the Type I arrivals during the transition to neap tides. Outside of the spring tides, the tidal cycles alternate between the small and medium bore amplitudes of Type II and Type III arrivals, just as the tidal height record alternates with the highs and lows of the daily inequality. Lastly, evidence of internal bore crossings are absent only on days of neap tides, as expected. Note that even if a few arrival pattern types have been misidentified by visual inspection, the basic patterns presented here would still exist.

V. LINEAR INVERSE METHODS

Section IV demonstrated how the acoustic record can be used to determine the presence or absence of internal bores and make general estimates of internal bore and internal tide amplitude from different tidal cycle types. However, acoustic data can also be used to estimate the subtle variations in several physical parameters among tidal cycles of the same type through the use of linear inverse methods. This section offers a demonstration of that technique using cases of spring tide (Type I) arrival structures. By varying the model's input parameters, one can calculate how a small perturbation to a modeled physical process, such as an increased tidal swing or internal bore amplitude, leads in the real acoustic data to small changes in acoustic travel times. Perturbing model parameters also helps quantify model stability and sensitivity. Because any single datum from the acoustic data can often be influenced by several physical processes simultaneously, inverse methods are used to determine how much each model parameter contributes to the total travel time perturbation.

TABLE II. Acoustic observables and uncertainties.

Observable	Description	Uncertainty
d_1	Upper/lower ray travel time separation at 1 h	1 ms
d_2	Upper/lower ray travel time separation at bore crossing	0.2 ms
d_3	Upper/lower ray travel time separation at 7 h	1 ms
d_4	Time of bore crossing	0.2 h
d_5	Time of upper ray disappearance	1.5 h
d_6	Time of upper ray reappearance	2 h
d_7	Duration of cloud of upper ray arrivals following bore crossing	1 h
d_8	Travel time separation in cloud of upper ray arrivals	1 ms

After observing how the real acoustic record varies with time, estimates can be made of how the physical processes of the Strait varied with time as well. Unfortunately, there are few simultaneous, independent environmental measurements to compare to the estimates calculated here, but comparisons to historical data are attempted when no direct observations are available. These estimates do provide examples of the variability in physical processes in the Strait, but because of the limited duration of the acoustic record, they are too short to serve as other than examples.

A. Sensitivity analysis

The model can help determine to which physical processes in the Strait of Gibraltar the acoustic transmissions are most sensitive, and learning how the predicted acoustic travel times vary with changing model parameters is a necessary step in the inverse calculation. In order to objectively measure travel time variability, acoustic features that could be measured on all spring tidal cycles were identified and will be called ''observables.'' The eight observables that were measured for each of 12 spring tidal cycles are described in Table II and identified in Fig. 10. Observables d_4, d_5, and d_6 are dependent upon placement of a 12 h window defining the start and end of a tidal cycle; they refer to times relative to a tidal cycle window, not an absolute time. For consistency, the times of the internal solitary wave crossings (d_4), seen in the acoustic data as the bottom of the upper ray travel time drop, were designated the 4 h mark for every tidal cycle window.

Figure 11 shows time series for seven of the eight acoustic observables listed in Table II in an effort to identify any trends over the seven days of spring tides. (Observable d_4, not shown, equals 4 h for all tidal cycles by definition, and in the inverse calculation to follow, it serves as a constraint on the time of the bore crossing.) Over this short time series, no strong trends are seen. Some of the variability is due in part to the difficulty in making the measurements.

It would be simplest if the sensitivity studies indicate

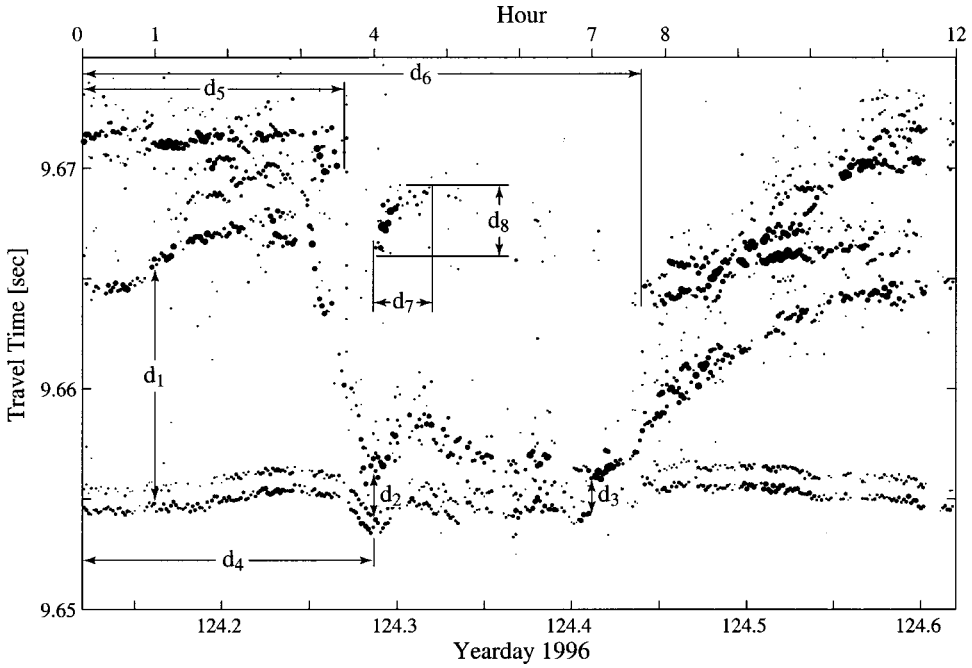

FIG. 10. Dimension lines illustrating the eight observables (d_1 through d_8) for a Type I arrival pattern. Observables are defined in Table II.

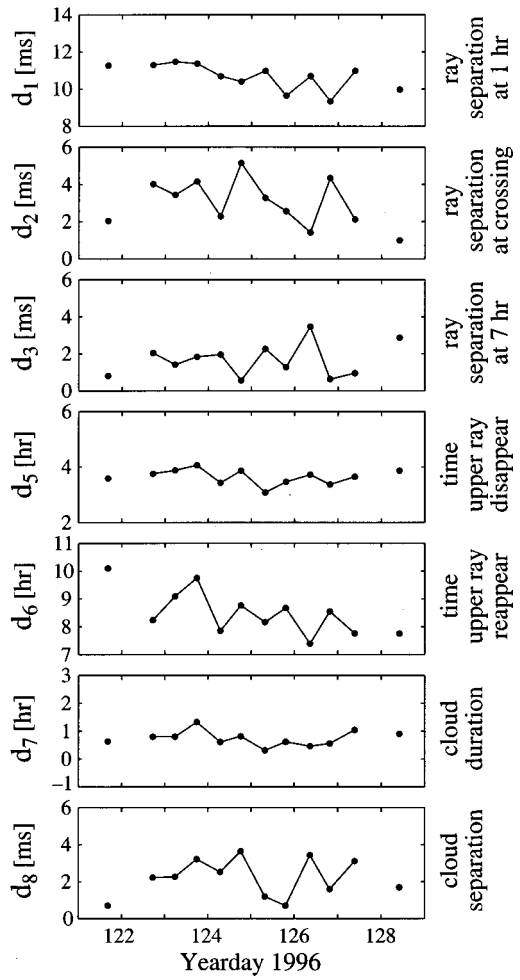

FIG. 11. Time series for seven observables from Type I arrivals. Data points from adjacent tidal cycles are connected by a line. Observables are defined in Table II.

that a travel time observable is affected by only a single model parameter, and thus the physical process that model parameter represents would be a good candidate for acoustic remote sensing. However, the inverse method is still able to provide model parameter estimates even when an observable is influenced by many parameters simultaneously, as is often the case here.

Eight model parameters were perturbed slightly, one at a time, in both a positive and negative direction from the reference state. The model was rerun after each perturbation and changes in the eight observables from the reference travel times were recorded. The result was a matrix of derivatives describing how each observable responds to perturbations in each model parameter. Table III lists all the model parameters along with the size of their perturbations. Perturbation sizes were chosen with the goal of being large enough to make a noticeable difference in travel time observables (about 0.5 ms or 0.5 h) but small enough so that the perturbations remained linear. If perturbed too far, eigenray paths change and some observables would no longer be measurable.

Because the internal bore amplitude is scaled with range across the Strait, perturbations to its associated model parameter, m_1, will be by a percentage of the reference state instead of an absolute number of meters. Model parameters m_3 and m_4, internal tide amplitude at the source and receiver, define the maximum and minimum for the range-dependent internal tide amplitude. Linearly interpolated between the endpoints, the internal tide amplitude is larger on the southern side of the Strait, near the source. The background sound-speed profiles can be offset vertically from their reference state, with the amount of offset interpolated linearly in range across the Strait between the values in m_5 and m_6, profile offsets at the source and receiver. This is equivalent to changing the depth and slope of the Atlantic/

TABLE III. Model parameter uncertainties and perturbations used in sensitivity studies.

Parameter	Description	Uncertainty	Perturbation (±)
m_1	Internal bore amplitude	12%	20%
m_2	Internal bore phase speed	0.5 m/s	0.3 m/s
m_3	Internal tide amplitude at source	12 m	10 m
m_4	Internal tide amplitude at receiver	10 m	10 m
m_5	Sound-speed profile vertical offset at source	8 m	10 m
m_6	Sound-speed profile vertical offset at receiver	8 m	10 m
m_7	Internal tide phase at source	0.12 rad	0.4 rad
m_8	Internal tide phase at receiver	0.12 rad	0.4 rad

Mediterranean interface. The tidal phase is also interpolated linearly in range across the Strait between the phase at the source and receiver, parameters m_7 and m_8. If the source and receiver phases are unequal, this makes the Atlantic/Mediterranean interface "rock" as the tide will at times be rising on one side of the acoustic path and falling on the other side.

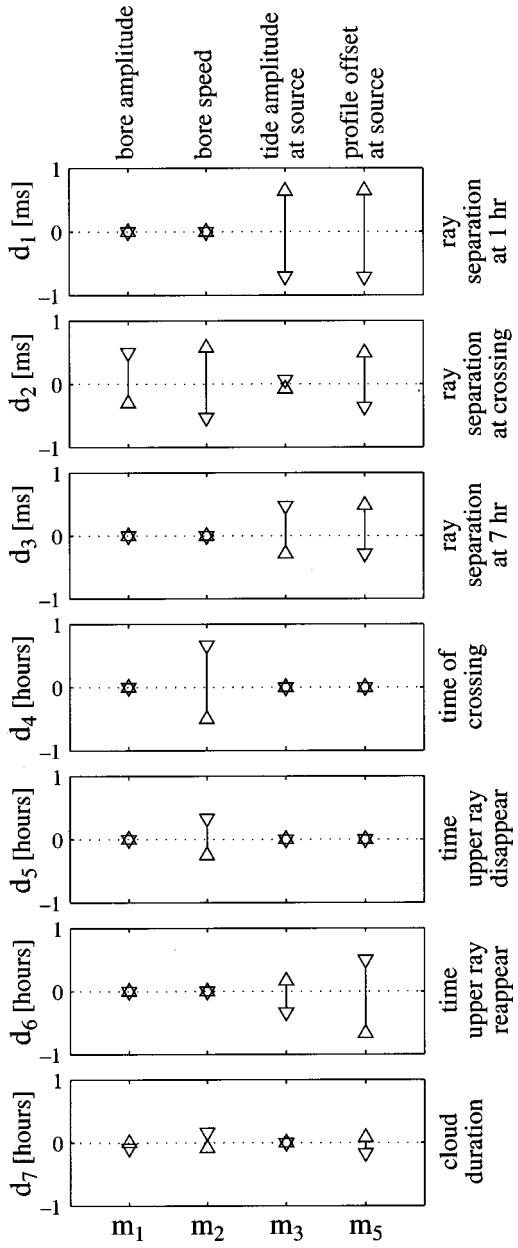

FIG. 12. Change in observable's (d_i) reference state in response to a model parameter (m_j) perturbation. For each observable/parameter combination, △ indicates the change due to a positive model parameter perturbation, and ▽ indicates a negative perturbation. Observables and model parameters are defined in Tables II and III.

When displayed graphically, linearity of the observables' derivatives with respect to model parameters ($\delta d_i / \delta m_j$) can quickly be verified and sensitivities to model parameters compared. Figure 12 shows a selected subset from the 8×8 matrix of derivatives. The changes to seven travel time observables, from both positive and negative perturbations to four model parameters, are shown. If the model reacts linearly to a perturbation, the changes to a travel time observable will be equal and opposite for the positive and negative perturbations. If a model parameter has no influence on an observable, its positive and negative derivatives will both be zero. For example, internal bore amplitude (m_1) has no effect on upper/lower ray travel time separation at the 1 h mark (d_1), but it does have an effect on upper/lower ray separation during the bore crossing (d_2). The relative strength with which a model parameter affects different observables can be compared by looking along any column of Fig. 12. For example, internal tide amplitude at the source (m_3) has a larger influence on observable d_1 than on any other observable.

While the impact of model parameter perturbations can be described numerically by the derivatives calculated above, enough was previously learned of the acoustic scattering to provide a qualitative explanation of why the acoustic observables change as they do. Figure 3 shows the modeled evolution of sound-speed profiles along the acoustic path, and the eigenray paths that result, at several times during a tidal cycle. Figure 3 will be referred to in the descriptions to follow, and the qualitative descriptions can be confirmed with the values shown in Fig. 12.

1. Internal bore amplitude

In Fig. 3, Hour 4, the presence of the internal bore over the source (T1) and receiver (T3) causes large sound-speed gradients which refract all upper rays ("c") down deep, paralleling the lower ray ("a"). If m_1, the internal bore amplitude, is increased, sound-speed gradients increase and all upper rays will be refracted even deeper, more closely following the lower ray. Because upper rays follow almost the same path as the lower ray, their travel times are nearly identical, and the observable d_2, upper/lower ray travel time separation at the bore crossing, decreases. Internal bore amplitude affects the fewest number of observables because

the internal bores are over the acoustic path for only a short time.

2. Internal bore phase speed

Changing the modeled phase speed of the internal bore mainly affects the timing of the upper ray travel time decrease and the disappearance of the late-arriving upper rays. Increasing m_2 causes the internal bore to pass over the acoustic path earlier and quicker, resulting in a decrease in the observable d_4, time of the bore crossing. An internal bore over the source also deflects the shallowest ray away from the shallowest sound channel, as seen in Fig. 3, Hour 2.58. This effect happens sooner with a faster bore, an effect measured by the observable d_5, the time of upper ray disappearance. The isolated clouds of upper ray arrivals at Hour 4.75 (''d'') are due to an internal bore over the receiver causing sound-speed gradients which refract shallow rays down on to the receiver from above. A slower moving internal bore will remain over the receiver for a longer time, thus increasing the duration of this effect. This increase is seen by observable d_7.

3. Internal tide amplitude

The model parameters m_3 and m_4 for internal tide amplitude dictate the maximum extent the background sound-speed profile will be shifted vertically over a tidal cycle. Comparing the soundspeed profiles of Fig. 3, Hour 1 and Hour 7 most clearly illustrates this shifting (after scaling by a vertical mode 1 function). Outside of Hours 2 to 5, changes in upper ray travel times are due to the internal tide's changes to the sound-speed field instead of from internal bore activity. As an upper ray will stay within the same sound channel over much of the tidal cycle, its path length changes as the sound channels shift vertically, thus changing its travel time. Lower ray travel times do not change significantly with the internal tide because sound-speed perturbations are small in deep water due to scaling by the vertical mode 1 function. An increased internal tide amplitude causes (at Hour 1) a larger upward vertical excursion by shallow sound channels, longer path lengths for that channel's eigenrays, and longer ray travel times. This is seen as in increase in observable d_1, upper/lower ray travel time separation at 1 h, since the upper ray takes longer to arrive but the lower ray travel time remains constant. During times of downward internal tide displacements (Hour 7), the sound channels carry rays into slightly faster water, thus decreasing a shallow ray's travel time and decreasing observable d_3. In all cases, observables seem more sensitive to internal tide amplitude changes on the source (southern) end of the acoustic path than at the receiver end. This may be because the source is shallower than the receiver and often within the double minimums of the sound-speed profiles where sound-speed gradients are stronger.

4. Sound-speed profile offset

The model parameters for adding a constant vertical offset to the background sound-speed field, m_5 and m_6, affect observables similarly to parameters of internal tide amplitude. The profile offset parameter defines a constant vertical shift to be added to the sinusoidal shifting defined by the internal tide parameters. Interestingly, parameter m_5, the profile offset at the source, has a large effect on observable d_6, the reappearance time of the late-arriving upper rays, while parameter m_6 has no effect. The reappearance of the upper ray arrivals indicates that the shallowest sound channel is once again being used. Rays refract up into the shallow sound channel immediately after leaving the source only when the source is below the deeper sound-speed minimum. This happens sooner when profiles at the source are offset shallower, and thus observable d_6 decreases.

In most cases the observables respond linearly to perturbations of a single model parameter; some may show a slightly unequal response to the positive and negative perturbation for a given parameter. Their successful use in an inverse calculation also requires that their responses be linear when several model parameters are perturbed simultaneously. Fortunately, the derivatives of the observables did add linearly when tested with several combinations of perturbations to internal tide amplitude, profile offset, tidal phase, and bore amplitude. However, testing the linearity for every combination of eight model parameters before proceeding with the inverse calculation was not feasible. It was assumed that the observables would behave linearly provided that model perturbations were small, and this was tested and confirmed in calculations using the new model parameter estimates provided by the inverse.

B. Linear inverse calculation

The sensitivity studies confirm that most observables are dependent upon more than one model parameter; observable d_5, time of shallow ray disappearance, is the only exception. When many observables change from their reference state simultaneously, inverse techniques can estimate what combination of model parameter perturbations will provide output that most closely matches the observables. The following matrices are used in the inverse calculation (Wunsch, 1996):

- d Data vector. For each of 12 spring tidal cycles, the difference between observables predicted for the reference state and measured observables.
- G Derivatives $(\delta d_i/\delta m_j)$ as measured in the sensitivity studies.
- R Data uncertainty covariance matrix. The diagonal of this matrix is the expected uncertainty for each observable, shown in Table II.
- P Model parameter uncertainty covariance matrix. The diagonal of this matrix guides how far the inverse is allowed to perturb each model parameter. Values are shown in Table III.

Once the above matrices are defined, they can be used in the inverse equation (1) to calculate $\hat{m}$, estimates of the amount to perturb each model parameter in order to match the data from each tidal cycle:

$$\hat{m} = (G^T R^{-1} G + P^{-1})^{-1} G^T R^{-1} d. \quad (1)$$

Uncertainties for the $\hat{m}$ estimates are calculated as follows:

$$\hat{P} = (G^T R^{-1} G + P^{-1})^{-1}. \quad (2)$$

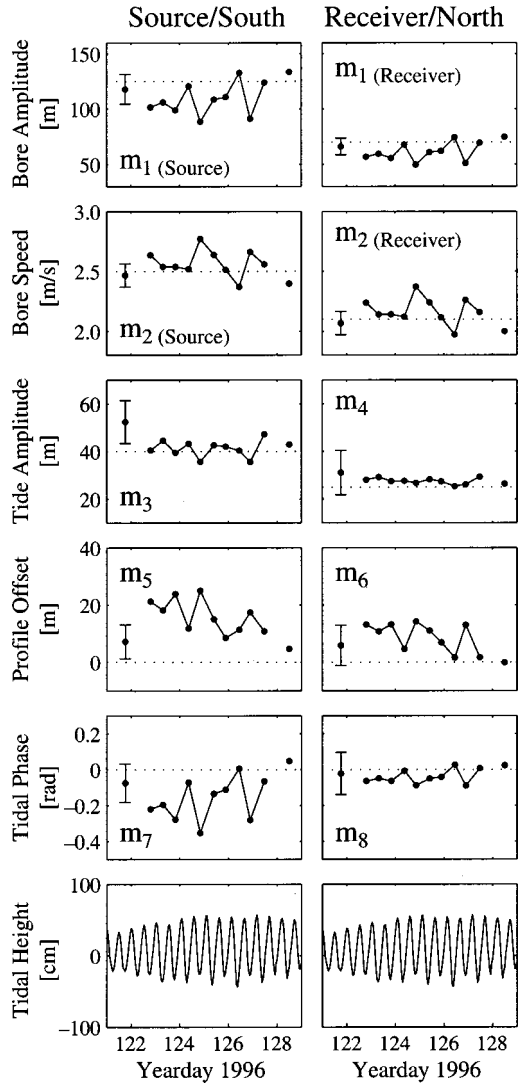

FIG. 13. Time series for eight corrected model parameters (m_j), plus the tidal height record from Ceuta. The uncertainty for each parameter is independent of yearday and shown only on the first data point. Data points from adjacent tidal cycles are connected by a solid line. Dotted lines indicate the model parameter value for the reference state. Model parameters are defined in Table III.

The precision with which the observations were required to match the model output depended on both the precision of the data (observation error) and the ability of the model to reproduce the observable (representation error). The uncertainty assigned to a given observable has variance that is the sum of the variance of the observational and representational error. While observational error was similar for most observables, representational error varied greatly, and dominated the uncertainties in matrix *R*. Observables that could be reproduced well in spite of the limited parameterization of the inverse model were given smaller uncertainties, thus requiring the inverse to match them more closely. In assigning values for the data error uncertainty matrix, the smallest uncertainties were given to d_2 and d_4, the observables from the time of the bore crossing.

The difference between the measured and modeled values for an observable is the residual, and the least square inverse procedure more strongly penalizes residuals for observables with small expected uncertainties. The inverse solution ($\hat{m}$) was optimized to have a low data misfit penalty while also minimizing the weighted magnitudes of the model parameter perturbations. The estimated model parameter perturbations were added to the reference model parameters to make corrected model parameters. Time series for the corrected model parameters, and thus the physical processes they represent, are shown in Fig. 13. Parameters m_1 and m_2 are not specific to the source or receiver side of the acoustic path as the other parameters are. However, they have been scaled per the range-dependent functions used in the model (detailed in Tiemann *et al.*, 2001) before being presented in Fig. 13. Error bars showing the standard deviations of the model parameter estimates are independent of yearday and are shown on the first data point only.

Despite the short time series available, some conclusions can be drawn. There is more variability in physical processes on the source (southern) side of the acoustic path than on the receiver (northern) side, but in most cases, perturbations at the source and receiver are in the same direction for a given parameter. The estimated internal bore amplitude, m_1, is usually smaller than the reference case, and as predicted from the sensitivity studies, it moves exactly opposite the time series for observable d_2, upper/lower ray separation at the time of the bore crossing. Observable d_2 would be the best choice to use in quickly estimating internal bore strength. The estimates of internal tide amplitude are consistent with historic observations that internal tides are larger on the southern side of the Strait, but it is unfortunate that the error bars for the tidal amplitude at the receiver are so relatively large. The tidal phase estimates suggest that the internal tides at the source and receiver should not be exactly in phase. As the Atlantic/Mediterranean interface depth rises and falls with the internal tide, the northern side is slightly ahead of the southern side, causing the interface to rock. This rocking was also seen in environmental data from three moorings, parallel to the acoustic path, measured concurrently with the Gibraltar experiment's acoustic data (B. Baschek, personal communication). The estimates of sound-speed profile offsets are equivalent to a change in the reference interface depth, and they might be used to measure the changing thickness of the Atlantic and Mediterranean water layers.

While the time series of Fig. 13 show no obvious trends with the tidal height record, their fluctuations and uncertainties give insight into how variable the physical processes in the Strait are, even over such a short time period. More obvious trends might be seen in longer series through both spring and neap tides or when compared to other processes such as the size of the hydraulic jump at the Camarinal Sill or the current flow through the narrows. This demonstration of the linear inverse calculation also confirms the model's stability and hopefully the usefulness of acoustic remote sensing. In recalculations of the forward problem using newly estimated model parameters, the model responds well to changes of multiple parameters simultaneously, providing reasonable matches to many spring tide arrivals and not just the one pattern to which it was originally fit.

VI. DISCUSSION

The Gibraltar experiment was designed to test the feasibility of using acoustic methods to measure physical oceanographic processes in an environment difficult for conventional instruments. The opportunity for rapid sampling in time, inherent integration in space, and ability to measure several physical parameters simultaneously and nonintrusively are key advantages of using acoustic techniques in the Strait of Gibraltar. This paper has offered demonstrations of a few techniques used to extract information from the acoustic record. More thorough environmental measurements would have been helpful in improving the model used in forward problem calculations and for verifying the acoustically derived estimates presented here. Long-term trends in the physical processes still need to be identified with a longer time series of data. The distribution of physical parameters is of interest as well; a longer time series of estimates could determine if the parameters behave as purely random variables.

As shown in Sec. IV, there were at least three different types of travel time arrival patterns observed during the few weeks of the experiment. Reproduction of those travel times assumed a mode 1 internal bore in every case, but with varying amplitudes. Armi and Farmer (1988) reported seeing some mode 2 internal bores in the narrows of the Strait in addition to numerous observations of mode 1 bores, and so the use of acoustic methods to determine the modal content of a passing bore was briefly investigated as well. The model was modified to scale the internal bore amplitude with a vertical mode 2 function, instead of the usual mode 1 function, and predicted acoustic travel times over a spring tidal cycle were recalculated. According to the model, a mode 2 bore would have caused acoustic rays to refract sharply down as they left the source, reflecting first off the sea floor and then the sea surface, but missing the receiver for 2 h out of the tidal cycle. As there is a continuous record of travel times recorded at the T3 receiver, it is possible that there were no instances of a mode 2 bore, especially since the three different types of arrival patterns can be explained using mode 1 bores of varying amplitude. However, the model may be tuned to work only with mode 1 bores as there is no other environmental data showing occurrences of mode 2 internal bores.

It has been suggested from studies of satellite images of the Strait that most internal solitary wave packets entering the Mediterranean Sea can be identified as either Northeast or Southeast Modes, named for their tendency to propagate in the directions indicated (Apel, 2000). Furthermore, there is evidence that the packets may alternate modes on a semidiurnal basis. If the Northeast and Southeast Modes have horizontal wave-fronts with significantly different shapes as they cross the acoustic path, that might also help explain the alternating Type II and Type III arrival structures seen in the acoustic data.

Lastly, this work has offered examples where acoustic remote sensing has not only confirmed previous observations of physical processes in the Strait but also offered some new insight and questioned historic understanding. For example, the average 5.4 h measured here for an internal bore to travel from the Camarinal Sill to the T1–T3 acoustic path agrees with Armi and Farmer's estimates (1988). This work has also confirmed that an internal bore passes through the narrows on average every 12.56 h with the semidiurnal tide. However, this brief acoustic record suggests that successive bore occurrences typically alternate longer and shorter than the mean spacing, increasing in variability with the daily inequality. The amplitude of an internal bore is reported to vary with tidal height, being largest during the spring tides. This work confirmed that is generally true when classifying tidal cycles according to their acoustic arrival pattern; the Type I patterns occur during the spring tides and are modeled with largest internal bore amplitudes of the three arrival types. However, this work suggests that internal bore amplitude does not always scale linearly with tidal height. Rather, during spring to neap tide transitions, it alternates between small and medium sized internal bores on adjacent tidal cycles, as seen in the ordering of Type II and Type III arrival pattern occurrences.

ACKNOWLEDGMENTS

U. Send was the principal investigator for the Gibraltar Acoustic Monitoring Experiment at the University of Kiel. B. Baschek provided analysis of the environmental data taken during the experiment. T. Birdsall and K. Metzger designed the 2 kHz signals and signal processing. M. Dzieciuch assisted with the data analysis. D. Farmer and L. Armi participated in many helpful discussions during the design and analysis of the experiment. The first phase of the field work was conducted with the able assistance of the crew of the German research vessel F/S POSEIDON. The Camarinal Sill mooring (S) was installed and data provided by J. Candela and D. Limeburner. The 2 kHz instruments were recovered by the Spanish Naval research vessel MALASPINA, which was generously made available to us by the Spanish Navy, with J. Rico (Instituto Hidrografico de la Marina, Cádiz, Spain) as Chief Scientist. The acoustic instrumentation was designed, fabricated, tested, and fielded by L. Day, K. Hardy, D. Horwitt, D. Peckham, and A. Rivera. B. Betts prepared the illustrations. This work was supported by the Office of Naval Research (ONR Grant No. N00014-95-1-0072) and the European Community MAST program (EC MAST-3 Contract No. MAS3-CT96-0060). C. Tiemann was supported by an ONR AASERT grant (ONR Grant No. N00014-95-1-0795).

Alpers, W., and La Violette, P. (**1993**). ''Tide-generated nonlinear internal wave packets in the Strait of Gibraltar observed by the synthetic aperture radar aboard the ERS-1 satellite,'' in *Proc. of the First ERS-1 Symposium, Eur. Space Agency Spec. Publ. ESA-SP 359(2)*, edited by B. Kaldeich (ESA Publications Division, Noordwijk, The Netherlands), pp. 753–758.

Apel, John R. (**2000**). ''Solitons near Gibraltar: Views from the European Remote Sensing Satellites,'' Data Report 2000-1, Global Ocean Associates, Silver Spring, Maryland.

Armi, L., and Farmer, D. M. (**1988**). ''The flow of Mediterranean water through the Strait of Gibraltar,'' Prog. Oceanogr. **21**, 1–105.

Boyce, F. (**1975**). ''Internal waves in the Straits of Gibraltar,'' Deep-Sea Res. **22**, 597–610.

Bray, N., Winant, C., Kinder, T., and Candela, J. (**1990**). ''Generation and kinematics of the internal tide in the Strait of Gibraltar,'' in *The Physical Oceanography of Sea Straits*, edited by L. Pratt (Kluwer Academic, Dordrecht), pp. 477–491.

Bray, N., Ochoa, J., and Kinder, T. (**1995**). ''The role of the interface in exchange through the Strait of Gibraltar,'' J. Geophys. Res. **100**, 10755–10776.
Candela, J., Winant, C., and Ruiz, A. (**1990**). ''Tides in the Strait of Gibraltar,'' J. Geophys. Res. **95**, 7313–7335.
Farmer, D. M., and Armi, L. (**1988**). ''The flow of Atlantic water through the Strait of Gibraltar,'' Prog. Oceanogr. **21**, 1–105.
Richez, C. (**1994**). ''Airborne synthetic aperture radar tracking of internal waves in the Strait of Gibraltar,'' Prog. Oceanogr. **33**, 93–159.
Send, U., Worcester, P. F., Cornuelle, B. D., Tiemann, C. O., and Baschek, B. (**2001**). ''Integral measurements of mass transport and heat content in straits from acoustic transmissions,'' Deep-Sea Res. (in press).
Tiemann, C. O., Worcester, P. F., and Cornuelle, B. D. (**2001**). ''Acoustic scattering by internal solitary waves in the Strait of Gibraltar,'' J. Acoust. Soc. Am. **109**, 143–154.
Watson, G., and Robinson, I. (**1990**). ''A study of internal wave propagation in the Strait of Gibraltar using shore-based marine radar images,'' J. Phys. Oceanogr. **20**, 374–395.
Watson, G. (**1994**). ''Internal waves in a stratified shear flow: The Strait of Gibraltar,'' J. Phys. Oceanogr. **24**, 509–517.
Wunsch, C. (**1996**). *The Ocean Circulation Inverse Problem* (Cambridge University Press, New York).
Ziegenbein, J. (**1970**). ''Spatial observations of short internal waves in the Strait of Gibraltar,'' Deep-Sea Res. **17**, 867–875.